Journal of Hazardous Materials xxx (xxxx) xxxx

Contents lists available at ScienceDirect

Journal of Hazardous Materials

journal homepage: www.elsevier.com/locate/jhazmat

Colorimetric aptasensor for ochratoxin A detection based on enzyme-induced gold nanoparticle aggregation

Yue He[a,b,c,*], Fengyu Tian[a,b,c], Jing Zhou[a,b,c], Qiyang Zhao[a,b,c], Ruijie Fu[a,b,c], Bining Jiao[a,b,c,*]

[a] Citrus Research Institute, Southwest University, Chongqing, 400712, PR China
[b] Laboratory of Quality & Safety Risk Assessment for Citrus Products (Chongqing), Ministry of Agriculture, PR China
[c] National Citrus Engineering Research Center, Chongqing, 400712, PR China

GRAPHICAL ABSTRACT

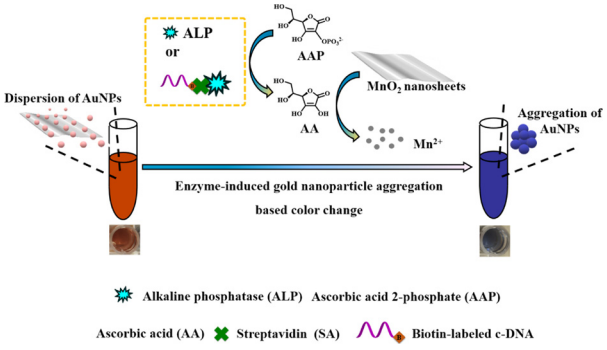

ARTICLE INFO

Editor: R. Teresa

Keywords:
Aptamer
Biosensor
Mycotoxins
Gold nanoparticle
Alkaline phosphatase

ABSTRACT

An innovative colorimetric method based on enzyme-induced gold nanoparticle aggregation was developed to detect the activity of alkaline phosphatase (ALP), and it was further applied to construct an aptasensor to monitor ochratoxin A (OTA) concentrations. In the presence of ALP, the substrate ascorbic acid 2-phosphate was hydrolyzed to generate ascorbic acid (AA). Subsequently, reduction of MnO_2 nanosheets by AA produced manganese ions, which mediated gold nanoparticle aggregation. The color of the detection solution changed from brown–red to purple to blue as the ALP concentration increased, and a detection limit of 0.05 $U{\cdot}L^{-1}$ was achieved. Furthermore, this strategy was successfully utilized to devise a target-responsive aptasensor for colorimetric detection of an important mycotoxin, OTA, which causes food poisoning and has various toxic effects on humans. The proposed method offers high sensitivity with a detection limit as low as 5.0 nM together with high specificity. When applied to analyze red wine and grape juice samples, no complex sample pretreatment or bulky instruments were required. Overall, a colorimetric platform based on enzyme-induced gold nanoparticle aggregation was successfully established to improve the simplicity and sensitivity of ALP and OTA detection. This platform appears highly promising for mycotoxin-related food safety monitoring.

* Corresponding authors at: Citrus Research Institute, Southwest University, Chongqing, 400712, PR China.
E-mail addresses: yuehe@cric.cn (Y. He), jiaobining@cric.cn (B. Jiao).

https://doi.org/10.1016/j.jhazmat.2019.121758
Received 25 September 2019; Received in revised form 8 November 2019; Accepted 24 November 2019
0304-3894/ © 2019 Elsevier B.V. All rights reserved.

1. Introduction

Colorimetric assay has been considered a powerful tool for determining component contents because of its exclusive advantages, such as easy operation, cost-effectiveness, and intuitive results. (Liu et al., 2019; Tang and Li, 2017) Due to these advantages, it has been widely adopted in point-of-care and on-site testing. (Shen et al., 2012; Chan et al., 2016) Enzyme-linked immunosorbent assay (ELISA), as one of the most popular colorimetric methods, has been extensively used in clinical diagnosis and hazardous materials monitoring. (Lequin, 2005) However, conventional horseradish peroxidase (HRP)-based ELISA methods using TMB-H_2O_2 system as signal readout is not suitable in resource-limited area detection. The reason lies in that it is difficult for the human eye to distinguish one color with different intensities. Gold nanoparticles (AuNPs), as one of the most ideal colorimetric indicators, have been received considerable attention by combing them with conventional ELISA platform because they offer low cost, easy preparation, ultra-high molar extinction coefficients, and distinct localized surface plasmon resonance (LSPR) properties. (Daniel and Astruc, 2004) The composition, size, shape, and aggregation state of AuNPs are particularly important factors that can induce a significant change in the LSPR and subsequently cause significant color changes that can be easily visualized by the naked eye. (Jain et al., 2006; Sun and Xia, 2002) Strategies involving metallization, etching, and aggregation of AuNPs are commonly used to modulate the LSPR of AuNPs. (Ma et al., 2016; Elghanian et al., 1997; Satija et al., 2016; Xuan et al., 2016) Among these strategies, colorimetric methods based on enzyme-induced aggregation of AuNPs have been actively studied for applications involving determination of small molecules, (Liang et al., 2018; Huang et al., 2016; Chen et al., 2018) biomarkers, (Zhang et al., 2015a; Yang and Tseng, 2016), and microorganisms (Xianyu et al., 2014; Nie et al., 2014; Xianyu et al., 2015) because of their low cost, high sensitivity, simple operation, and sufficient signal intensity for naked eye detection. For example, Liang et al. utilized hydroxyl radicals from HRP-catalyzed H_2O_2 to polymerize tyramine. This polymerization realized aggregation of AuNPs. Based on this, an immunosensor was developed for ochratoxin A (OTA) detection. (Liang et al., 2018) Xianyu et al. reported a colorimetric immunosensor based on an alkaline phosphatase (ALP)-mediated click reaction between azide- and alkyne-functionalized AuNPs to induce aggregation of AuNPs for determining immunoglobulin G. (Xianyu et al., 2014) Nie et al. used acetylcholinesterase to hydrolyze acetylthiocholine to achieve aggregation of AuNPs. (Nie et al., 2014) This method exhibited extraordinarily high sensitivity toward *Treponema pallidum*, which was three orders of magnitude higher than that of a conventional enzyme-linked immunosorbent assay (ELISA). Although color changes generated by enzyme-induced aggregation of AuNPs can lead to high sensitivity and selectivity toward target molecules, the use of antibodies as recognition elements restricts the practical applications of these immunocolorimetric methods. This is due to the poor stability of the antibodies and their complex and time-consuming preparation and functionalization, which increase the cost of the method. (Liu et al., 2009) Therefore, aptamers, as an emerging class of molecules that offer high stability, target versatility, easy synthesis, easy modification, and low cost, are becoming increasingly attractive. (Famulok et al., 2007) Consequently, it is essential to devise a novel colorimetric assay based on enzyme-induced aggregation of AuNPs by utilizing aptamers as alternatives to antibodies. As far as we know, a colorimetric aptasensor based on enzyme-induced aggregation of AuNPs has not yet been reported.

With these insights, herein, we propose a simple and sensitive colorimetric aptasensor based on enzyme-induced aggregation of AuNPs for OTA detection. ALP has been selected as a model enzyme, because it can specifically hydrolyze the dephosphorylation of various substrates. (Coleman, 1992) Owing to its high hydrolysis efficiency, versatile substrate specificity, and good stability, ALP has been used to establish various biosensors as readout enzymes. (Zhang et al., 2015a; Tian et al., 2019; Yang et al., 2015; Sun et al., 2016; Zhang et al., 2015b) Hence, effectively monitoring the activity of ALP is not only directly useful for diagnosing ALP-related diseases (Millan and Whyte, 2016; Saif et al., 2005) but also facilitates the development of ALP-based biosensors. Additionally, it has been reported that salt-mediated AuNP aggregation offers high sensitivity in colorimetric signal generation. (Han et al., 2011; Saha et al., 2012) For example, based on the interaction between Mn^{2+} and dopamine, Mn^{2+} can cause the aggregation of AuNPs. (Narayanan and Park, 2014) Especially, metal oxide-based nanomaterials such as CoOOH nanoflakes, (Liu et al., 2018) MnO_2 nanoparticles, (Fu et al., 2018) and MnO_2 nanosheets (Wang et al., 2019) can produce abundance metal ions after decomposition. Among these metal oxide-based nanomaterials, the preparation process of MnO_2 nanosheets has the advantages of cost-effectiveness, simple operation process and easy access to raw materials. (Deng et al., 2011) Therefore, MnO_2 nanosheets have become an ideal ion source to develop new colorimetric methods based on salt-mediated AuNP aggregation strategy. Therefore, the principle of our proposed colorimetric strategy is the use of ALP to hydrolyze ascorbic acid 2-phosphate (AAP) to ascorbic acid (AA), which can reduce MnO_2 nanosheets to Mn^{2+}, thereby inducing aggregation of AuNPs, which can lead to vivid color changes in the sensing system. This strategy was further expanded to construct an aptasensor by using ALP as a readout enzyme. OTA was selected as a model target. The ALP activity directly corresponded to the OTA concentration via an aptamer structure switching reaction on magnetic beads (MBs). Based on this strategy, the presence of OTA was expected to produce a color change via enzyme-induced aggregation of AuNPs. This strategy not only provides an easily used platform for detecting ALP, which has broad potential in the clinical diagnosis of ALP-related diseases, but also explores a new type of colorimetric aptasensor for OTA, which is meaningful for food quality and safety assurance.

2. Experimental section

2.1. Materials and apparatus

A biotin-labeled OTA aptamer, 5′-biotin-AAAAAAAAAAAAGATCG GGTGTGGGTGGCGTAAAGGGAGCATCGGACA-3′, a biotin-labeled partially complementary DNA strand of the aptamer, 5′-biotin-AAAAAAA AAAAATGTCCGATGCT-3′, and 5′-FAM-AAAAAAAAAAAATGTCCGAT GCT-3′ were all prepared by Shanghai Sangon Biotechnology Co., Ltd. (Shanghai, China). Streptavidin–alkaline phosphatase (SA–ALP) was provided by Vector Laboratories, Inc. (Burlingame, USA). ALP was obtained from Takara Biotechnology Co., Ltd. (Dalian, China). All the mycotoxins were obtained from Pribolab Pte. Ltd. (Singapore). The mycotoxins included OTA, zearalenone (ZEA), ochratoxin B (OTB), aflatoxin B1 (AFB1), tenuazonic acid (TeA), alternariol (AOH), altenuene (ALT), and citrinin. Streptavidin magnetic beads (SA-MBs) with a diameter of 1 μm were provided by New England Biolabs, Inc. (New England). Manganese chloride tetra hydrate ($MnCl_2{\cdot}4H_2O$), tetramethylammonium hydroxide (TMA·OH), AA, and AAP were purchased from Sigma-Aldrich, Inc. (Shanghai, China). Bovine serum albumin (BSA), human serum albumin (HSA), acid phosphatase (ACP), and reduced glutathione (GSH) were all purchased from Shanghai Sangon Biotechnology Co., Ltd. (Shanghai, China). Para-nitrophenyl phosphate (pNPP) was supplied by Beyotime Biotechnology Co. (China). OliGreen (OG) was purchased from ThermoFisher Scientific (USA). Buffer A was used to prepare ALP-DNA-immobilized MBs consisting of 20 mM Tris − HCl (pH 7.4), 100 mM NaCl, and 5 mM $Mg(Cl)_2$. An ALP reaction buffer was used in the experiment, which consisted of 20 mM Tris − HCl (pH 8.0), and 5 mM $Mg(Cl)_2$. A Millipore Milli-Q water purification system was used to prepare 18.2 MΩ cm deionized water. Absorption spectra were measured with a Varioskan LUX microplate reader (Vantaa, Finland). Transmission electron microscopy (TEM) images were acquired with a JEM-1200EX transmission electron microscope (JEOL, Tokyo). X-ray photoelectron spectroscopy (XPS)

characterization was performed with Thermo ESCALAB 250Xi spectrometer (USA). The hydrodynamic diameter of AuNPs were measured by a dynamic light scattering (DLS) instrument (Zetasizer Nano). Inductively coupled plasma mass spectrometry (ICP-MS, Agilent 7800ce) was used to quantify the manganese ion concentration of the samples. The experimental data were analyzed with Origin 9.0.

2.2. Synthesis of AuNPs

AuNPs were synthesized according to a method developed by Natan et al. (Grabar et al., 1995) Significantly, all glassware was thoroughly washed with aqua regia (HCl/HNO_3, 3:1, v/v) and deionized water. Particularly, 100 mL of 1.0 mM $HAuCl_4$ solution was heated to boiling, and magnetically stirred. Subsequently, 1 mL of 400 mM sodium citrate solution was rapidly added to the above solution. The mixed solution was kept boiling and stirred for 10 min. After cooling to room temperature, citrate-stabilized AuNPs (13 nm) were obtained. It was reported that the extinction coefficient for AuNPs (13 nm) at 520 nm was $2.7 \times 10^8\ M^{-1}\ cm^{-1}$. (Demers et al., 2000) Together with the absorption intensity of AuNPs at 520 nm, the AuNP concentration was calculated.

2.3. Synthesis of MnO_2 nanosheets

According to a previously developed method, (Zhao et al., 2014) MnO_2 nanosheets were synthesized. Specifically, 800 μL TMA·OH (15 M) and 2 mL H_2O_2 (30 %) were mixed. The above mixed solution was then diluted to 20 mL with deionized water. Subsequently, 10 mL 0.3 M $MnCl_2$ was rapidly added. The mixture was stirred vigorously for 12 h at room temperature, and a dark brown color was observed. By thoroughly washing the above solution with deionized water, bulk MnO_2 was obtained. This was then ultrasonicated for 2 h to obtain ultra-thin MnO_2 nanosheets. The extinction coefficient of MnO_2 nanosheets at 380 nm was reported as $9.6 \times 10^3\ M^{-1}\ cm^{-1}$. (Liu et al., 2017) Together with the absorption intensity of MnO_2 nanosheets at 380 nm, the MnO_2 nanosheets concentration was calculated.

2.4. Preparation of ALP-DNA-immobilized MBs

ALP-DNA-immobilized MBs were directly prepared according to our previous report. (Tian et al., 2019) Firstly, SA-MBs were thoroughly washed with buffer A. Subsequently, 4 μL biotin-labeled aptamer (100 μM) was added and incubated for half an hour at room temperature with gentle shaking. Through removing separate biotin-labeled aptamer by washing thrice with buffer A, the aptamer-immobilized MBs were formed; 4 μL biotin-labeled cDNA (100 μM) was then added, followed by incubating for half an hour at room temperature. Similarly, by washing thrice with buffer A, the separate biotin-labeled cDNA was removed. Finally, 4 μL SA–ALP (1 mg/mL) was added and mixed well for half an hour at room temperature. After washing five times with ALP reaction buffer, excess SA–ALP was removed. Finally, the prepared ALP-DNA-immobilized MBs were stored in a refrigerator for further use. The loading amount of the ALP on the MBs and the homogeneity of the loading of ALP, and the clarification of the hybridization between biotin-labeled cDNA and biotin-labeled aptamer, were discussed in the electronic supporting information (ESI, supporting discussions and Figs. S1, S2, S3, and S4).

2.5. Colorimetric detection of ALP

For ALP detection, 20 μL of various ALP concentrations in Tris－HCl buffer were mixed with 4 μL of 10 mM AAP. The mixture was incubated at 37 °C for half an hour. Then, 136 μL of double-distilled H_2O (ddH_2O), 10 μL of 0.4 mM MnO_2 nanosheets, and 30 μL of 6.7 nM AuNPs were added. After incubating at room temperature for 5 min, the absorption spectra were acquired with the microplate reader. Each ALP concentration was tested thrice.

To investigate the specificity of ALP-mediated aggregation of AuNPs, BSA, HSA, GSH, and AA were tested instead of ALP under the conditions used for ALP detection. Three replicates of each molecular analysis were performed to calculate the error bars.

2.6. Colorimetric detection of OTA

For quantitative OTA measurement, various OTA concentrations from 6.25 nM to 12,500 nM were reacted with 20 μL of the ALP-DNA-immobilized MBs for half an hour at room temperature. The solution was then separated with a magnetic scaffold. The supernatant (20 μL) was used in the following experimental steps to achieve ALP-mediated aggregation of AuNPs. Each OTA concentration was tested thrice. The whole assay time was estimated to be 70 min, which is comparable to the conventional ELISA method (1～2 h).

2.7. Detection of OTA under complex environment

Grape juice and red wine samples were obtained from the local supermarket. OTA was then added to these authentic samples and detected with the enzyme-mediated colorimetric method involving aggregation of AuNPs described above. It should be noted that, because of the acidity of the grape juice and the red wine, pH was corrected prior to the beginning of the procedure. Specifically, 8 μL of 1 M sodium hydroxide was added to 1 mL of 20 % grape juice to adjust of the pH. And, 4 μL of 1 M sodium hydroxide was added to 1 mL of 10 % red wine to correct the pH. Then, 10 μL of various OTA concentrations spiked in 20 % grape juice and 10 % red wine were reacted with 20 μL of the ALP-DNA-immobilized MBs for half an hour at room temperature. After magnetic separation, 20 μL of supernatant were mixed with 4 μL of 10 mM AAP. The mixture was incubated at 37 °C for half an hour. Then, 136 μL of double-distilled H_2O (ddH_2O), 10 μL of 0.4 mM MnO_2 nanosheets, and 30 μL of 6.7 nM AuNPs were added. After incubating at room temperature for 5 min, the absorption spectra were acquired with the microplate reader. The final OTA concentrations changed from 6.25 nM to 12,500 nM. Each OTA concentration was tested thrice.

3. Results and discussion

3.1. Sensing mechanism

Fig. 1A shows the mechanism of the colorimetric strategy based on enzyme-induced aggregation of AuNPs. In the absence of ALP, AAP was unable to reduce MnO_2 nanosheets. Under these circumstances, the mixture of AuNPs and MnO_2 nanosheets appeared brown–red. When ALP was present, AAP was cleaved into phosphate anions and a reducing agent, AA, which reduced the MnO_2 nanosheets to Mn^{2+}. After incubating the produced Mn^{2+} with AuNPs, Mn^{2+} interacted with carboxyl groups on the surface of the AuNPs, resulting in aggregation of the AuNPs, which led to a color change in the solution. To demonstrate the feasibility of this method, the UV–visible (UV–vis) spectral properties of this system were investigated. As shown in Fig. 1B, inset a, AuNPs (1 nM) appeared wine-red in ddH_2O and showed a characteristic SPR absorption peak around 520 nm (Fig. 1C, curve a). As the catalytic ALP reaction required a slightly alkaline buffer with a certain concentration of metal ions, we investigated the color and spectrum of AuNPs in 10 % ALP reaction buffer. As shown in Fig. 1B, inset b, the AuNPs appeared purple under these conditions with a decreased absorption peak at 520 nm and a broad absorption peak at a higher wavelength (Fig. 1C, curve b). This indicated slight aggregation of AuNPs. On introducing MnO_2 nanosheets (0.02 mM) to 10 % ALP reaction buffer, the AuNPs appeared brown–red (Fig. 1B, inset d), unlike the color of AuNPs in 10 % ALP reaction buffer (purple, Fig. 1B, inset b) and MnO_2 nanosheets (light brown, Fig. 1B, **inset c**). Together, an increased absorption at the whole UV–vis region and an absorption peak

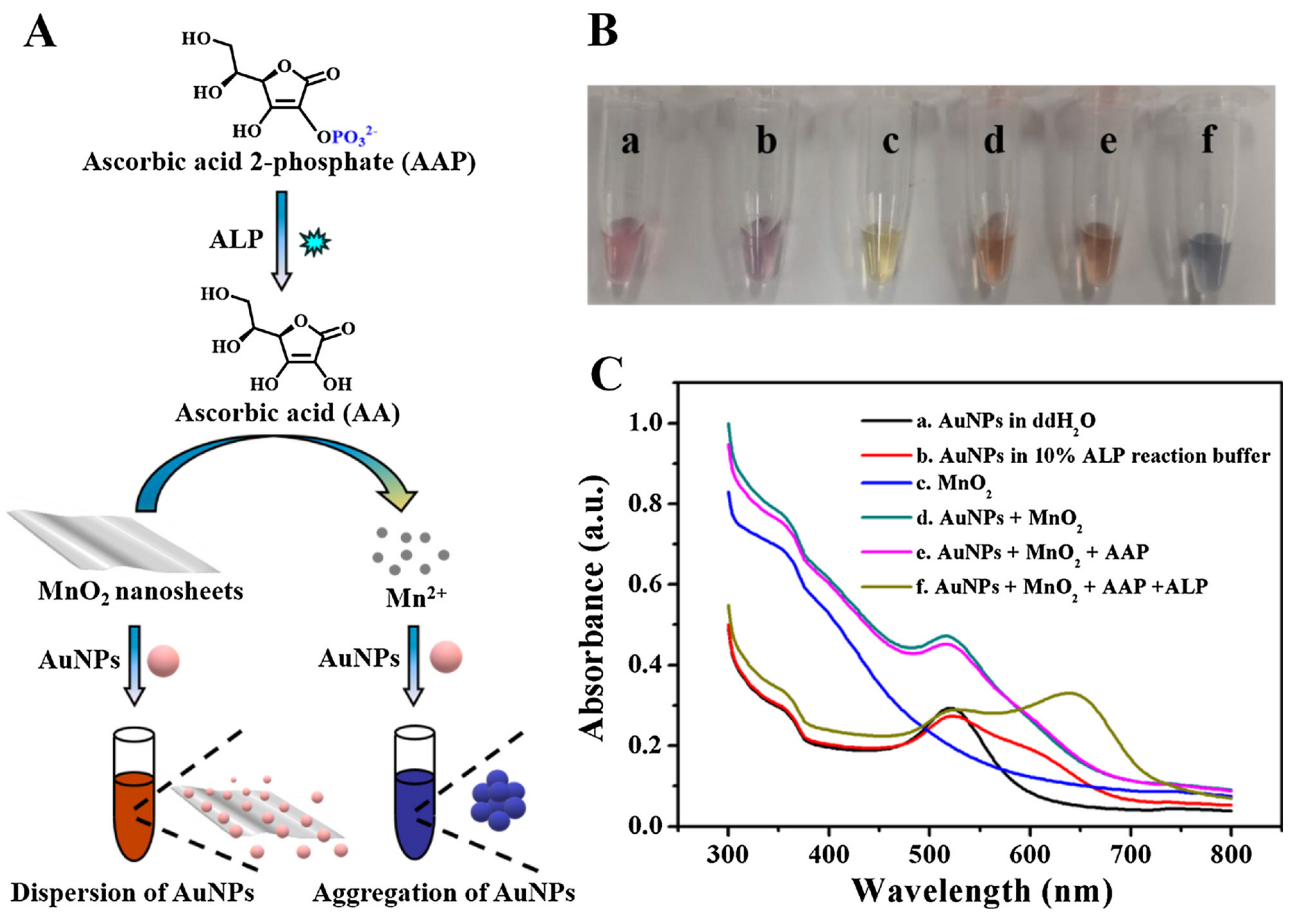

Fig. 1. (A) Schematic of colorimetric assay involving enzyme-induced aggregation of AuNPs. (B) Photograph corresponding to (a) AuNPs in ddH_2O, (b) AuNPs in 10 % ALP reaction buffer, (c) MnO_2 nanosheets, (d) AuNPs + MnO_2 nanosheets, (e) AuNPs + MnO_2 nanosheets + AAP, and (f) AuNPs + MnO_2 nanosheets + AAP + ALP. (C) Corresponding absorption spectra of above solutions. AuNPs, 1 nM; MnO_2 nanosheets, 0.02 mM; AAP, 0.2 mM; ALP, 150 $U{\cdot}L^{-1}$.

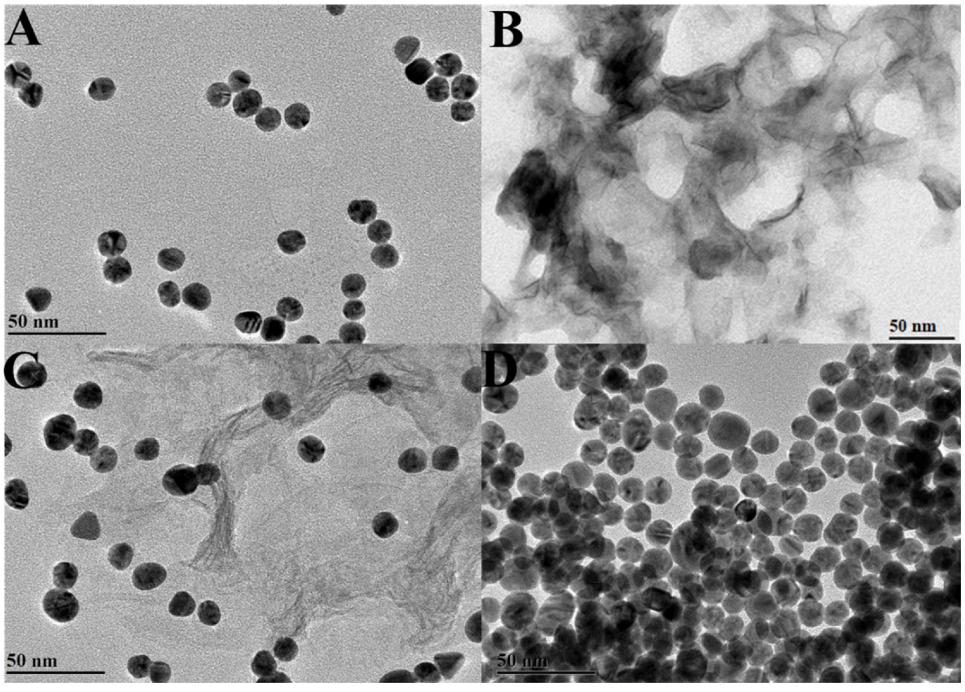

Fig. 2. TEM images of (A) AuNPs, (B) MnO_2 nanosheets, (C) AuNPs + MnO_2 nanosheets, and (D) AuNPs + MnO_2 nanosheets + (AAP + ALP).

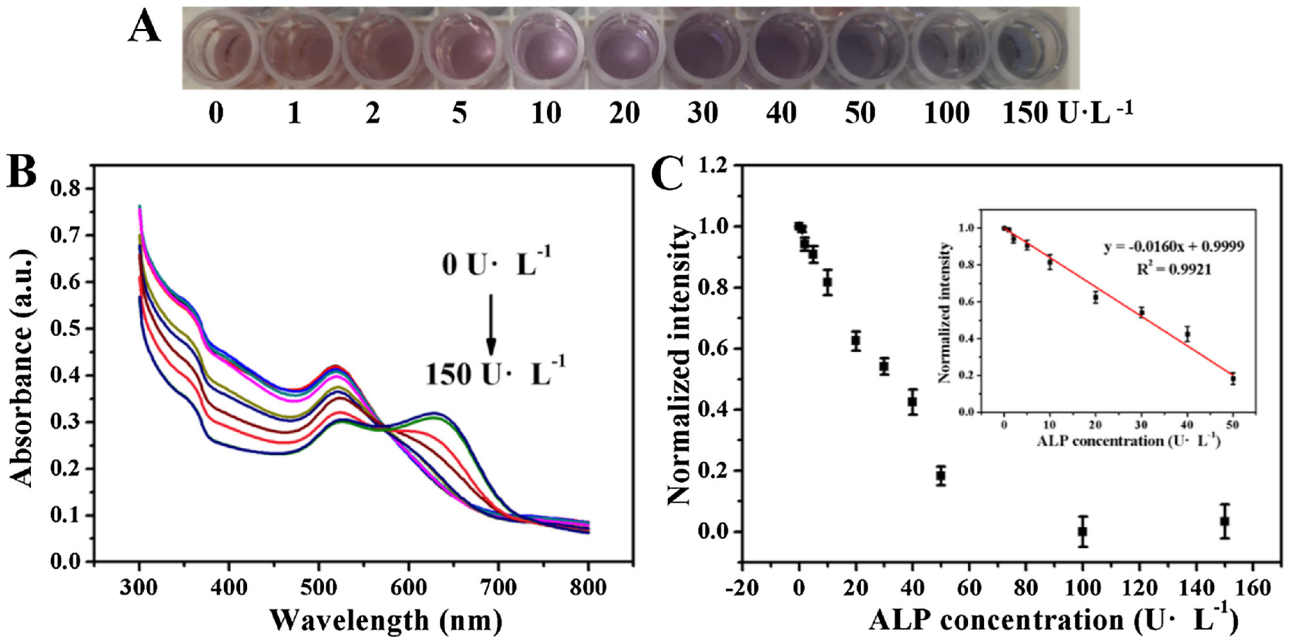

Fig. 3. (A) Visual photograph of semi-quantitative determination of ALP. (B) UV–vis absorption spectra in the presence of different ALP concentrations. (C) The relationship between the normalized absorption intensity at 520 nm versus the ALP concentration. AuNPs, 1 nM; MnO_2 nanosheets, 0.02 mM; AAP, 0.2 mM. Standard deviations of three repeated measurements were used to calculate the error bars.

at 520 nm was observed (Fig. 1C, curve d). This may be attributed to their own absorption of MnO_2 nanosheets (Fig. 1C, curve c) in the UV–vis region, coupled with the protective effect of MnO_2 nanosheets toward AuNPs. Furthermore, based on the principle of this method, the aggregation of AuNPs caused by Mn^{2+} was demonstrated. As shown in Fig. S5, curve a, distinct changes in the color and absorbance of AuNPs were observed after incubation with the mixture of AA and MnO_2 nanosheets. The Mn^{2+} concentration produced by the reaction between AA and MnO_2 nanosheets was measured by ICP-MS as 0.125 mM. As shown in Fig. S5, curve b, the same phenomenon was observed after incubating AuNPs with 0.125 mM Mn^{2+} as when incubating AuNPs with the mixture of AA and MnO_2 nanosheets, which indicated that aggregation of AuNPs was caused by Mn^{2+}. Fig. 1B, inset e, and C, curve e, show that without ALP, AAP (0.2 mM) had minimal influence on the color and spectrum of AuNPs in a solution of MnO_2 nanosheets. However, after adding ALP, the solution appeared obviously blue (Fig. 1B, inset f), and the absorption peak of the solution at 520 nm decreased significantly, with a maximum absorption peak appearing at 650 nm (Fig. 1C, curve f). XPS was used to demonstrate the decomposition of MnO_2 nanosheets by the generating AA from ALP-catalyzed AAP hydrolysis reaction. (Ilton et al., 2016) As shown in Fig. S6A, the binding energy of the high resolution XPS spectrum of the Mn 2p regions at 653.5 eV for Mn 2p 1/2, and 644.8 and 641.9 eV for Mn 2p 3/2 are matched well with the oxidation state for Mn(IV). However, after reaction with the catalyzed product of ALP, the 2p 3/2 satellite at 646.4 eV was appeared (Fig. S6B). This is only assigned to the satellite for Mn (II). Therefore, we can conclude that MnO_2 nanosheets were reduced by the generating AA from ALP-catalyzed AAP hydrolysis reaction. This conclusion was further verified by the Mn3 s peaks, which are normally used to distinguish the oxidation states of Mn. As displayed in Fig. S7, a separation energy of 4.8 and 6.0 eV of Mn 3 s were obtained, which are corresponded to Mn(IV) and Mn(II), respectively. Through above XPS spectra, the MnO_2 nanosheets were successfully reduced and converted to Mn^{2+}. All these results together confirmed the mechanism of the enzyme-induced aggregation of AuNPs. The process of enzyme-induced aggregation of AuNPs was further confirmed by the TEM results. As shown in Figs. 2A and S8, the AuNPs exhibited a monodisperse and uniform spherical morphology with an average size of 13.4 ± 1.5 nm. The MnO_2 nanosheets presented a representative two-dimensional sheet-like morphology with the lateral size of several hundreds of nanometers (Fig. 2B). After mixing these two nanomaterials, separated AuNPs and an integrated AuNPs/MnO_2 assembly could be clearly seen (Fig. 2C). Meanwhile, the energy dispersive X-ray elemental mapping images of the mixed solution of AuNPs and MnO_2 nanosheets were further performed to confirm the presence of Au, Mn and O element after the mixing process (Fig. S9). However, after adding ALP to catalyze the hydrolysis of AAP, the AuNPs aggregated (Fig. 2D). This phenomenon was further confirmed by the size distributions of the AuNPs by DLS. As shown in Fig. S10, AuNPs in the sensing system with ALP exhibited a unimodal size distribution of 440.2 ± 13.6 nm, which is much larger than the AuNPs in deionized water (13.8 ± 0.3 nm), owing to the ALP-induced aggregation of AuNPs. These results demonstrate the feasibility of ALP detection.

3.2. Optimization of assay conditions

To achieve an excellent ALP detection performance, the concentrations of MnO_2 nanosheets and AAP were optimized. The absorption spectra of AuNPs in the absence and presence of ALP with different concentrations of MnO_2 nanosheets are shown in Fig. S11A and B, respectively. The change in A_{650}/A_{520} ($\triangle(A_{650}/A_{520}) = (A_{650}/A_{520}) - (A_{650}/A_{520})_0$) was used to achieve the optimization, where (A_{650}/A_{520}) and $(A_{650}/A_{520})_0$ are the ratios of the absorbance at 650 nm to that at 520 nm in the presence and absence of ALP, respectively. Fig. S11C shows the influence of various concentrations of MnO_2 nanosheets on $\triangle(A_{650}/A_{520})$. When the concentration of MnO_2 nanosheets was 0.02 mM, $\triangle(A_{650}/A_{520})$ peaked. A photograph of AuNPs in the absence and presence of ALP with various concentrations of MnO_2 nanosheets is shown in Fig. S11D. At a concentration of 0.02 mM, there was a significant difference between the color of AuNPs in the absence and presence of ALP, which further demonstrated that 0.02 mM of MnO_2 nanosheets was the optimum concentration. Therefore, 0.02 mM MnO_2 nanosheets was utilized for follow-up experiments. As the substrate for ALP, AAP could significantly influence the amount of AA production. Therefore, the AAP concentration should be carefully optimized. As shown in Fig. S12A, as the AAP concentration increased, the absorption

intensity at 520 nm gradually decreased, while it was enhanced at 650 nm. The inset of Fig. S12A shows that the AuNP solutions changed from brown–red to blue, clearly corresponding to the absorption spectra as the AAP concentration increased from 0 to 0.2 mM; thereafter, almost no changes were observed, illustrating that the maximum degree of aggregation of AuNPs was achieved. These results were also confirmed by the A_{650}/A_{520} result, as A_{650}/A_{520} reached a plateau when using 0.2 mM AAP (Fig. S12B). Therefore, the optimal AAP concentration was 0.2 mM.

3.3. Application of colorimetric detection of ALP

The performance of the colorimetric method for ALP activity was studied under the above optimized conditions. As shown in Fig. 3A, the solution color changed significantly from brown–red to purple to blue as the ALP concentration increased. This indicated that naked eye semi-quantitative analysis of ALP through an enzyme-induced AuNP aggregation-based color change can be easily realized, thus providing an extremely convenient method of detecting ALP. Similarly, the absorption intensity decreased at 520 nm, while it gradually increased at 650 nm (Fig. 3B). This demonstrated that AuNPs gradually aggregated, corresponding to the image in Fig. 3A, as the ALP concentration increased. Simultaneously, the normalized absorption intensity at 520 nm (A_{norm}), which was calculated as $A_{norm} = (A_{520} - A_{min})/(A_{max} - A_{min})$, where A_{max} and A_{min} represent the maximum and minimum absorption intensities at 520 nm, respectively, has a good linear relationship with the ALP concentration between 1 and 50 $U{\cdot}L^{-1}$. The linear function was $y = -0.0160x + 0.9999$ (y represents A_{norm} and x represents the ALP concentration), with $R^2 = 0.9921$. The performance for ALP detection was comparable or slightly superior to those of previous detection methods (**Table S1**). This could be attributed to enzyme-mediated signal amplification.

To evaluate the selectivity, BSA, HSA, ACP, GSH, and AA were used as negative samples. As illustrated in Fig. 4A, the absorption spectrum showed that the absorption intensity at 650 nm increased remarkably and decreased at 520 nm only in the group with ALP. However, BSA, HSA, and ACP gave the opposite results. This may be attributed to their own absorption in the UV–vis region, coupled with the protective effect of these proteins toward AuNPs (Figs. S13 and S14). It is noteworthy that GSH and AA induced an increase in the absorption intensity at 650 nm. This may be because the reducing ability of GSH and AA promotes the degradation of MnO_2 nanosheets, leading to aggregation of the AuNPs. Furthermore, the normalized absorption intensity at 520 nm with different molecules is shown in Fig. 4B. There is a significant difference between ALP and the other biological species. ALP exhibited a minimum normalized intensity compared with the other molecules. Additionally, in contrast to the color (blue) of the solution with ALP, BSA, HSA, and ACP induced a brighter brown–red color, while GSH and AA induced minimal color changes. These results indicated that the proposed enzyme-induced colorimetric method involving aggregation of AuNPs can be applied to detect ALP with high specificity.

3.4. Application of colorimetric detection of OTA

Subsequently, we expanded this enzyme-induced colorimetric assay involving aggregation of AuNPs to construct an aptasensor for mycotoxin assay. OTA was used as a model analyte, because it is an important mycotoxin that shows strong nephrotoxicity, immunotoxicity, hepatotoxicity, mutagenicity, teratogenic toxicity, neurotoxicity, and carcinogenicity. (Petzinger and Ziegler, 2000; Malir et al., 2013; Sorrenti et al., 2013) OTA is listed as a potential human carcinogen (Group 2B) by the International Agency for Research on Cancer (IARC) as it is widespread and harmful to humans. (Pfohl-Leszkowicz and Manderville, 2007) Therefore, establishing fast and sensitive OTA detection techniques is critical for food safety. (Guo et al., 2011; Lv et al., 2017, 2016; Lv et al., 2018)

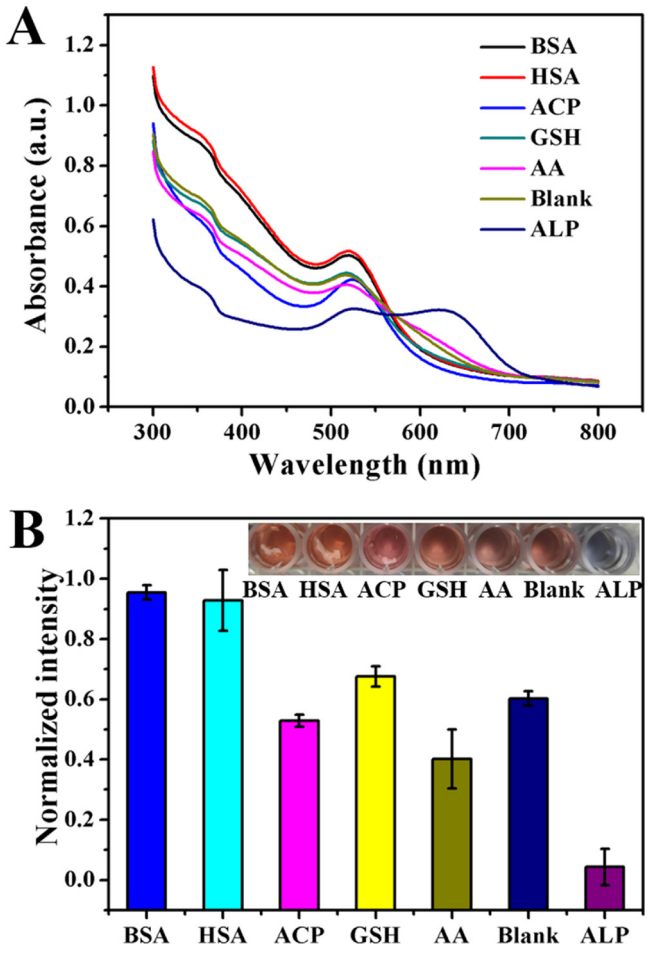

Fig. 4. (A) Absorption spectra of the colorimetric sensor with BSA (10 μM), HSA (10 μM), ACP (10 μM), GSH (10 μM), AA (10 μM), and ALP (150 $U{\cdot}L^{-1}$). (B) Histogram of the normalized absorption intensity at 520 nm for the above molecules. Inset: the corresponding photograph. AuNPs, 1 nM; MnO_2 nanosheets, 0.02 mM; AAP, 0.2 mM. Standard deviations of three repeated measurements were used to calculate the error bars.

As shown in Fig. 5A, DNA-ALP-immobilized MBs, which were prepared as described in our previous report, (Tian et al., 2019) were used for OTA detection. They were modified with an OTA aptamer, biotinylated cDNA, and SA–ALP. Specifically, after the aptamer of OTA immobilized on MBs, the biotinylated cDNA hybridized with aptamer to form an aptamer–cDNA duplex. Subsequently, with the introduction of SA–ALP, DNA-ALP-immobilized MBs were prepared. In the presence of OTA, OTA bound to its aptamer. As a result, the structure of the aptamer switched from an aptamer–cDNA duplex to an aptamer–OTA complex. Consequently, ALP-cDNA was liberated from DNA-ALP-immobilized MBs. After magnetic separation, the strategy involving enzyme-induced aggregation of AuNPs was initiated by ALP converting AAP to the reducing agent AA. Subsequently, MnO_2 nanosheets could be easily reduced by AA, inducing abundant Mn^{2+} production, leading to aggregation of AuNPs. Sequentially, an obvious color change in the AuNP solutions could be observed. Therefore, OTA could be expediently detected by the naked eye. Fig. 5B shows the color change in the solution with different OTA concentrations, which can be easily observed with the naked eye. As the OTA concentration increased, the solution changed from brown–red to purple to blue. Meanwhile, the absorption intensity at 520 nm decreased, while increasing at 650 nm, as the OTA concentration increased (Fig. 5C). Fig. 5D shows a good linear relationship between the normalized intensity at 520 nm and the OTA concentration from 6.25–750 nM, with the linear equation $y = -8.316 \times 10^{-4}x + 0.9994$, where y represents A_{norm} and x represents

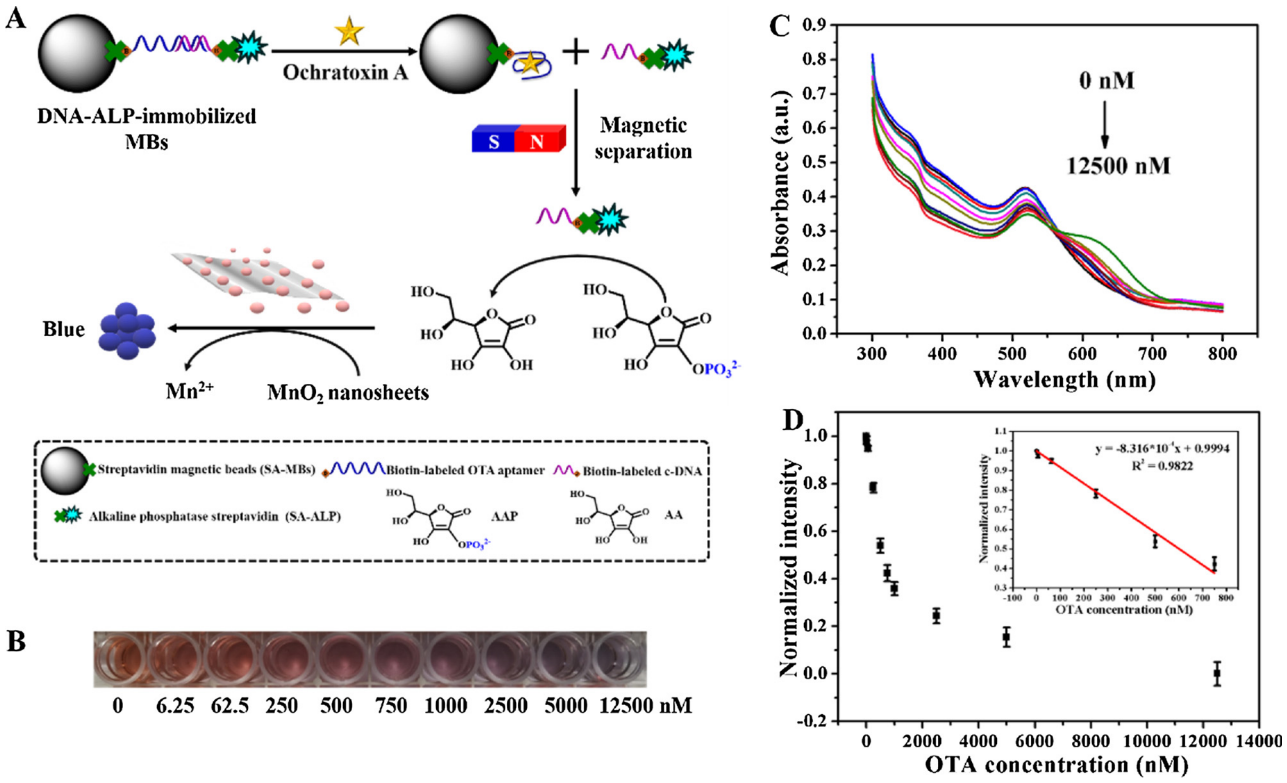

Fig. 5. (A) Schematic of the mechanism of colorimetric aptasensor based on enzyme-induced aggregation of AuNPs for OTA detection. (B) Visual photo of semi-quantitative determination of OTA. (C) UV–vis absorption spectra in the presence of different OTA concentrations. (D) The relationship between the normalized absorption intensity at 520 nm versus different OTA concentrations. AuNPs, 1 nM; MnO_2 nanosheets, 0.02 mM; AAP, 0.2 mM. Standard deviations of three repeated measurements were used to calculate the error bars.

the OTA concentration. The detection limit was calculated as 5.0 nM (2 μg/kg) based on a signal-to-noise ratio of 3 dividing the slope of the calibration curve. The European Commission has set the maximum tolerated OTA levels in various foods, for instance, 5 μg/kg for cereal grains, 5 μg/kg for roasted coffee, and 2 μg/kg for wine and grape juice. (Badie Bostan et al., 2017) This result indicated that the proposed aptasensor could be successfully satisfied the maximum tolerable OTA by low. Furthermore, this aptasensor for OTA determination is comparable with the majority of reported colorimetric methods (**Table S2**). When compared with the conventional ELISA kits, the cost of this aptasensor is a little cheaper (～USD $2.5566 for a single test) (**Table S3 and S4**). Importantly, this enzyme-induced AuNPs aggregation strategy, involving ALP activity to reflect the concentration of OTA. The excellent performance for OTA detection demonstrates high efficiency of ALP hydrolyzing AAP in the method. Moreover, this enzyme-induced AuNPs aggregation strategy, which was designed according to the structure switching of aptamers, has huge potential for the detection of other analytes by replacing of the corresponding aptamers.

To evaluate the specificity of the developed enzyme-induced colorimetric aptasensor based on aggregation of AuNPs, some common mycotoxins such as ZEA, citrinin, TeA, AOH, ALT, AFB1, and OTB were selected as negative controls. As shown in Fig. 6A, ZEA, citrinin, TeA, AOH, ALT, AFB1, and OTB induced negligible absorption changes, while OTA caused a significant decrease in absorption at 520 nm. A histogram of the normalized intensity of OTA and other mycotoxins at 520 nm is shown in Fig. 6B. The normalized intensity at 520 nm exhibited a significant difference between OTA and other mycotoxins. Meanwhile, as shown in the photograph inset of Fig. 6B, ZEA, citrinin, TeA, AOH, ALT, AFB1, and OTB induced negligible color changes, with the reaction solution remaining brown–red, while a significant color change was observed only in the presence of OTA. Therefore, this method could be applied for OTA detection with outstanding specificity.

Subsequently, grape juice and red wine were chosen to study the feasibility of the colorimetric method for targets analysis in complex matrix. As shown in Figs. S15 and S16, OTA with different concentrations still induced obvious color changes. It is noteworthy that, in grape juice matrix, OTA induced a color change from brown–red to red. No blue color was observed (Fig. S15A). This may be attributed to the protective effect of grape juice toward AuNPs. Accordingly, Fig. S15B shows that the absorption intensity at 520 nm still decreased as the OTA concentration increased. However, the absorption intensity at 650 nm did not increase. Nevertheless, there was still a good linear relationship between the normalized intensity at 520 nm and the OTA concentration from 6.25–750 nM compared with the performance of OTA detection in clean buffer and red wine. These results confirmed that the colorimetric aptasensor based on enzyme-induced aggregation of AuNPs could response OTA under complex environment with high sensitivity without complex pre-processing treatment or bulky equipment.

Next, with the above linear curves, the recoveries were determined by spiking grape juice and red wine with three different concentrations of OTA (200, 400, and 600 nM), respectively. **Table S5** displays the recoveries ranging from 99.4%–104.2, and the relative standard deviation (RSD) results were less than 2 %. To further evaluate the accuracy of the proposed method, chromatography tandem mass spectrometry (LC–MS/MS) method was established to measure the aforementioned three spiked grape juice samples and three spiked red wine samples. As shown in Fig. S17, the concentrations obtained with the proposed method and LC–MS/MS method are consistent with each other. These results indicate that the accuracy of our designed method is acceptable.

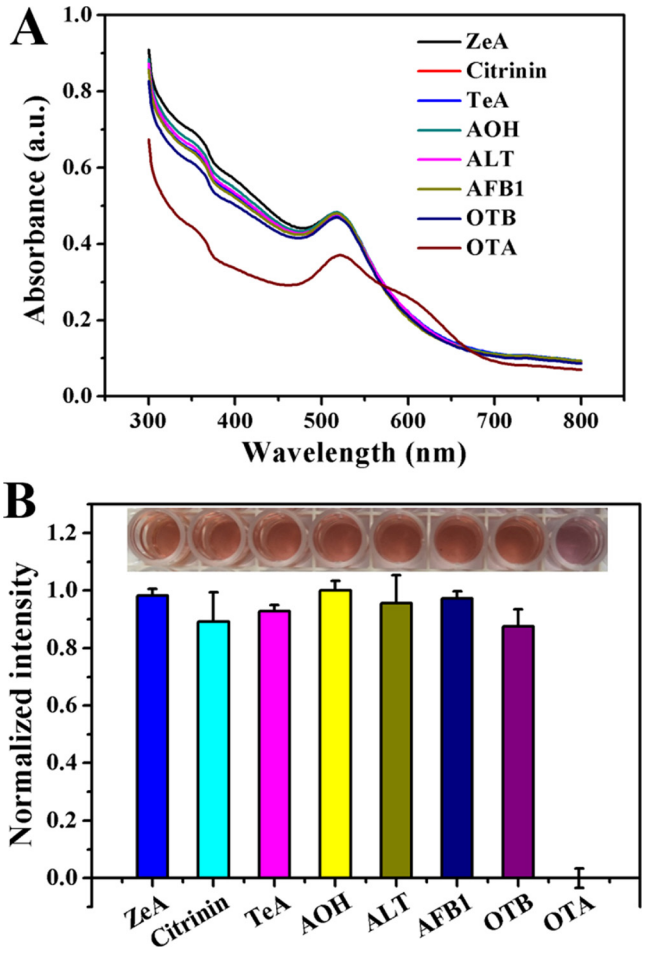

Fig. 6. (A) UV–vis absorption spectra of the colorimetric system with OTA and other mycotoxins. (B) Histogram of the normalized absorption intensity of at 520 nm for different mycotoxins. Inset: the corresponding photograph. AuNPs, 1 nM; MnO_2 nanosheets, 0.02 mM; AAP, 0.2 mM; mycotoxins, 750 nM. Standard deviations of three repeated measurements were used to calculate the error bars.

4. Conclusions

In summary, a colorimetric aptasensor based on enzyme-induced aggregation of AuNPs has been developed by combining the highly sensitive enzyme-mediated aggregation of AuNPs with the efficient binding ability of an aptamer toward OTA. By utilizing the advantages of the amplification effect of the catalytic ALP reaction and the outstanding sensitivity of aggregation of AuNPs to the ion concentration, OTA can be detected at a low concentration of 5.0 nM. Moreover, this colorimetric method was applied to grape juice and red wine matrix with satisfactory results. No complex sample pretreatment or bulky equipment were required. Therefore, this method offers broad prospects in food safety applications.

Declaration of Competing Interest

The authors declare that they have no known competing financial interests or personal relationships that could have appeared to influence the work reported in this paper.

Acknowledgments

The authors are grateful for the financial support of China Agriculture Research System (No. CARS-26), Natural Science Foundation Project of CQ (No. cstc2018jscx-msybX0263), Fundamental Research Funds for the Central Universities (No. XDJK2019C026), National Citrus Engineering Research Center (NCERC2019007) and National Risk Assessment Program for Agricultural Products Quality and Safety (No. GJFP2019012).

Appendix A. Supplementary data

Supplementary material related to this article can be found, in the online version, at doi:https://doi.org/10.1016/j.jhazmat.2019.121758.

References

Bostan, B.H., Danesh, N.M., Karimi, G., Ramezani, M., Shaegh, S.A.M., Youssefi, K., Charbgoo, F., Abnous, K., Taghdisi, S.M., 2017. Ultrasensitive detection of ochratoxin A using aptasensors. Biosens. Bioelectron. 98, 168–179.

Chan, H.N., Shu, Y.W., Xiong, B., Chen, Y.F., Chen, Y., Tian, Q., Michael, S.A., Shen, B., Wu, H.K., 2016. Simple, cost-effective 3D printed microfluidic components for disposable, point-of-care colorimetric analysis. ACS Sens. 1, 227–234.

Chen, X., Liang, Y., Zhang, W., Leng, Y.K., Xiong, Y.H., 2018. A colorimetric immunoassay based on glucose oxidase-induced AuNP aggregation for the detection of fumonisin B1. Talanta 186, 29–35.

Coleman, J.E., 1992. Structure and mechanism of alkaline-phosphatase. Annu. Rev. Bioph. Biom. 21, 441–483.

Daniel, M.C., Astruc, D., 2004. Gold nanoparticles: assembly, supramolecular chemistry, quantum-size-related properties, and applications toward biology, catalysis, and nanotechnology. Chem. Rev. 104, 293–346.

Demers, L.M., Mirkin, C.A., Mucic, R.C., Reynolds, R.A., Letsinger, R.L., Elghanian, R., Viswanadham, G., 2000. A Fluorescence-based method for determining the surface coverage and hybridization efficiency of thiol-capped oligonucleotides bound to gold thin films and nanoparticles. Anal. Chem. 72, 5535–5541.

Deng, R.R., Xie, X.J., Vendrell, M., Chang, Y.T., Liu, X.G., 2011. Intracellular glutathione detection using MnO_2-nanosheet-modified upconversion nanoparticles. J. Am. Chem. Soc. 133, 20168–20171.

Elghanian, R., Storhoff, J.J., Mucic, R.C., Letsinger, R.L., Mirkin, C.A., 1997. Selective colorimetric detection of polynucleotides based on the distance-dependent optical properties of gold nanoparticles. Science 277, 1078–1081.

Famulok, M., Hartig, J.S., Mayer, G., 2007. Functional aptamers and aptazymes in biotechnology, diagnostics, and therapy. Chem. Rev. 107, 3715–3743.

Fu, K., Zheng, Y., Li, J., Liu, Y., Pang, B., Song, X., Xu, K., Wang, J., Zhao, C., 2018. Colorimetric immunoassay for rapid detection of vibrio parahemolyticus based on Mn^{2+} mediates the assembly of gold nanoparticles. J. Agr. Food Chem. 66, 9516–9521.

Grabar, K.C., Freeman, R.G., Hommer, M.B., Natan, M.J., 1995. Preparation and characterization of au colloid monolayers. Anal. Chem. 67, 735–743.

Guo, Z., Ren, J., Wang, J., Wang, E., 2011. Single-walled carbon nanotubes based quenching of free FAM-aptamer for selective determination of ochratoxin A. Talanta 85, 2517–2521.

Han, X., Goebl, J., Lu, Z., Yin, Y., 2011. Role of salt in the spontaneous assembly of charged gold nanoparticles in ethanol. Langmuir 27, 5282–5289.

Huang, X., Chen, R., Xu, H., Lai, W., Xiong, Y., 2016. Nanospherical brush as catalase container for enhancing the detection sensitivity of competitive plasmonic ELISA. Anal. Chem. 88, 1951–1958.

Ilton, E.S., Post, J.E., Heaney, P.J., Ling, F.T., Kerisit, S.N., 2016. XPS determination of Mn oxidation states in Mn (hydr)oxides. Appl. Surf. Sci. 366, 475–485.

Jain, P.K., Lee, K.S., El-Sayed, I.H., El-Sayed, M.A., 2006. Calculated absorption and scattering properties of gold nanoparticles of different size, shape, and composition: applications in biological imaging and biomedicine. J. Phys. Chem. B 110, 7238–7248.

Lequin, R.M., 2005. Enzyme immunoassay (EIA)/enzyme-linked immunosorbent assay (ELISA). Clin. Chem. 51, 2415–2418.

Liang, Y., Huang, X., Chen, X., Zhang, W., Ping, G., Xiong, Y., 2018. Plasmonic ELISA for naked-eye detection of ochratoxin A based on the tyramine-H 2 O 2 amplification system, Sensor Actuat. B-Chem. 259, 162–169.

Liu, X., Huang, D., Lai, C., Qin, L., Zeng, G., Xu, P., Li, B., Yi, H., Zhang, M., 2019. Peroxidase-like activity of smart nanomaterials and their advanced application in colorimetric glucose biosensors. Small 15, 1900133.

Liu, J.W., Cao, Z.H., Lu, Y., 2009. Functional nucleic acid sensors. Chem. Rev. 109, 1948–1998.

Liu, S.G., Han, L., Li, N., Xiao, N., Ju, Y.J., Li, N.B., Luo, H.Q., 2018. A fluorescence and colorimetric dual-mode assay of alkaline phosphatase activity via destroying oxidase-like CoOOH nanoflakes. J. Mater. Chem. B 6, 2843–2850.

Liu, J., Meng, L., Fei, Z., Dyson, P.J., Jing, X., Liu, X., 2017. MnO_2 nanosheets as an artificial enzyme to mimic oxidase for rapid and sensitive detection of glutathione. Biosens. Bioelectron. 90, 69–74.

Lv, L., Li, D., Liu, R., Cui, C., Guo, Z., 2017. Label-free aptasensor for ochratoxin A detection using SYBR Gold as a probe. Sensor Actuat. B-Chem. 246, 647–652.

Lv, L., Cui, C., Liang, C., Quan, W., Wang, S., Guo, Z., 2016. Aptamer-based single-walled carbon nanohorn sensors for ochratoxin A detection. Food Control 60, 296–301.

Lv, L., Jin, Y., Kang, X., Zhao, Y., Cui, C., Guo, Z., 2018. PVP-coated gold nanoparticles for the selective determination of ochratoxin A via quenching fluorescence of the free aptamer. Food Chem. 249, 45–50.

ARTICLE IN PRESS

Ma, X., Chen, Z., Kannan, P., Lin, Z., Qiu, B., Guo, L., 2016. Gold nanorods as colorful chromogenic substrates for semiquantitative detection of nucleic acids, proteins, and small molecules with the naked eye. Anal. Chem. 88, 3227–3234.
Malir, F., Ostry, V., Novotna, E., 2013. Toxicity of the mycotoxin ochratoxin A in the light of recent data. Toxin Rev. 32, 19–33.
Millan, J.L., Whyte, M.P., 2016. Alkaline phosphatase and hypophosphatasia. Calcified Tissue Int. 98, 398–416.
Narayanan, K.B., Park, H.H., 2014. Colorimetric detection of manganese(II) ions using gold/dopa nanoparticles, Spectrochim. Acta A Mol. Biomol. Spectrosc. 131, 132–137.
Nie, X.M., Huang, R., Dong, C.X., Tang, L.J., Gui, R., Jiang, J.H., 2014. Plasmonic ELISA for the ultrasensitive detection of Treponema pallidum. Biosens. Bioelectron. 58, 314–319.
Petzinger, E., Ziegler, K., 2000. Ochratoxin A from a toxicological perspective. J. Vet. Pharmacol. Ther. 23, 91–98.
Pfohl-Leszkowicz, A., Manderville, R.A., 2007. Ochratoxin A: An overview on toxicity and carcinogenicity in animals and humans. Mol. Nutr. Food Res. 51, 61–99.
Saha, K., Agasti, S.S., Kim, C., Li, X., Rotello, V.M., 2012. Gold nanoparticles in chemical and biological sensing. Chem. Rev. 112, 2739–2779.
Saif, M.W., Alexander, D., Wicox, C.M., 2005. Serum alkaline phosphatase level as a prognostic tool in colorectal cancer: a study of 105 patients. J. Appl. Res. 5, 88–95.
Satija, J., Punjabi, N., Mishra, D., Mukherji, S., 2016. Plasmonic-ELISA: expanding horizons. RSC Adv. 6, 85440–85456.
Shen, L., Hagen, J.A., Papautsky, I., 2012. Point-of-care colorimetric detection with a smartphone. Lab Chip 12, 4240–4243.
Sorrenti, V., Di Giacomo, C., Acquaviva, R., Barbagallo, I., Bognanno, M., Galvano, F., 2013. Toxicity of ochratoxin a and its modulation by antioxidants: a review. Toxins 5, 1742–1766.
Sun, Y.G., Xia, Y.N., 2002. Shape-controlled synthesis of gold and silver nanoparticles. Science 298, 2176–2179.
Sun, J., Hu, T., Xu, X.L., Wang, L., Yang, X.R., 2016. A fluorescent ELISA based on the enzyme-triggered synthesis of poly (thymine)-templated copper nanoparticles. Nanoscale 8, 16846–16850.
Tang, L., Li, J., 2017. Plasmon-based colorimetric nanosensors for ultrasensitive molecular diagnostics. ACS Sens. 2, 857–875.
Tian, F., Zhou, J., Jiao, B., He, Y., 2019. A nanozyme-based cascade colorimetric aptasensor for amplified detection of ochratoxin A. Nanoscale.
Wang, J., Wang, D.X., Tang, A.N., Kong, D.M., 2019. Highly integrated, biostable, and self-powered DNA motor enabling autonomous operation in living bodies. Anal. Chem. 91, 5244–5251.
Xianyu, Y.L., Wang, Z., Jiang, X.Y., 2014. A plasmonic nanosensor for immunoassay via enzyme-triggered click chemistry. ACS Nano 8, 12741–12747.
Xianyu, Y., Chen, Y., Jiang, X., 2015. Horseradish peroxidase-mediated, iodide-catalyzed cascade reaction for plasmonic immunoassays. Anal. Chem. 87, 10688–10692.
Xuan, Z., Li, M., Rong, P., Wang, W., Li, Y., Liu, D., 2016. Plasmonic ELISA based on the controlled growth of silver nanoparticles. Nanoscale 8, 17271–17277.
Yang, Y.C., Tseng, W.L., 2016. 1,4-Benzenediboronic-acid-induced aggregation of gold nanoparticles: application to hydrogen peroxide detection and biotin–avidin-mediated immunoassay with naked-eye detection. Anal. Chem. 88, 5355–5362.
Yang, Z.H., Zhuo, Y., Yuan, R., Chai, Y.Q., 2015. Amplified thrombin aptasensor based on alkaline phosphatase and hemin/G-quadruplex-catalyzed oxidation of 1-naphthol. ACS Appl. Mater. Inter. 7, 10308–10315.
Zhang, Z.Y., Chen, Z.P., Wang, S.S., Cheng, F.B., Chen, L.X., 2015a. Iodine-mediated etching of gold nanorods for plasmonic ELISA based on colorimetric detection of alkaline phosphatase. ACS Appl. Mater. Inter. 7, 27639–27645.
Zhang, J., Xiang, Y., Novak, D.E., Hoganson, G.E., Zhu, J., Lu, Y., 2015b. Using a personal glucose meter and alkaline phosphatase for point-of-care quantification of galactose-1-phosphate uridyltransferase in clinical galactosemia diagnosis. Chem. Asian J. 10, 2221–2227.
Zhao, Z., Fan, H., Zhou, G., Bai, H., Liang, H., Wang, R., Zhang, X., Tan, W., 2014. Activatable fluorescence/MRI bimodal platform for tumor cell imaging via MnO_2 nanosheet-aptamer nanoprobe. J. Am. Chem. Soc. 136, 11220–11223.